Draft version February 5, 2008
Preprint typeset using LaTeX style emulateapj v. 6/22/04

HIGH REDSHIFT INTERGALACTIC C IV ABUNDANCE MEASUREMENTS FROM THE NEAR-INFRARED SPECTRA OF TWO $Z \sim 6$ QSOS [1]

Robert A. Simcoe[2,3]

Draft version February 5, 2008

ABSTRACT

New measurements of the $z \sim 6$ intergalactic C IV abundance are presented, using moderate resolution IR spectra of two QSOs taken with GNIRS on Gemini South. These data were systematically searched for high redshift C IV absorption lines, using objective selection criteria. Comprehensive tests were performed to quantify sample incompleteness, as well as the rate of false positive C IV identifications. The trend of constant $\Omega_{\rm C\ IV}(z)$ observed at $z \sim 2-5$ appears to continue to $z \sim 6$, the highest observed redshift. The C IV sample is also consistent with the redshift-invariant form of the C IV column density distribution reported by Songaila (2001) at lower redshift, although with fairly large uncertainties due to a smaller sample size and noisier infrared data. The constant value of $\Omega_{\rm C\ IV}$ does not necessarily imply that the IGM was infused with an early metallicity "floor," but the presence of early C IV does indicate that heavy-element enrichment began $\lesssim 1$ Gyr after the Big Bang. The lack of a decline in $\Omega_{\rm C\ IV}$ at high redshift may indicate that integrated C IV measurements are sensitive to the instantaneous rate of feedback from galaxy formation at each epoch. Alternatively, it could result from a balance in the evolution of the intergalactic gas density, ionization conditions, and heavy-element abundance over time.

Subject headings:

1. INTRODUCTION

Recent CMB measurements of the electron scattering optical depth suggest that star formation first began to ionize the IGM at $z \approx 11$, about 425 Myr after the Big Bang (Spergel et al. 2006). The subsequent epoch between $z = 11$ and the end of reionization at $z \sim 6$ (Fan et al. 2002; White et al. 2003; Djorgovski et al. 2001) encompasses only ~ 500 Myr. This interval begins to approach the dynamical timescale for massive galaxy formation and supernova feedback, so the galaxies formed at $z \sim 6-10$ may be among the first objects to produce the heavy elements seen in the IGM at $z \sim 3$ (Schaye et al. 2003; Simcoe et al. 2004).

If the large scale enrichment of the IGM actually began within this short window, one would expect to see either a significant downward trend in heavy-element abundances, or at least an increase in abundance scatter approaching $z \sim 5-6$. Even if the heavy elements are removed from early galaxies by strong winds, there are constraints on the distance that these winds will cover based simply on travel time (e.g. $D \sim 10$ kpc per 100Myr for a 100 km s^{-1}wind). It is also likely that early galactic winds would stall at $R \lesssim 100$ kpc because of mass loading from both the ISM and the IGM, which is $300-1000$ times more dense at these redshifts than in the present day.

To date, no abundance decline has been observed in the IGM towards high redshifts. Over the $z \sim 2-4$ range where one can estimate ionization-corrected carbon abundances from C IV , Schaye et al. (2003) found no significant redshift evolution in [C/H] across a sample of several sightlines. Likewise, Songaila (2001, 2005) and Pettini et al. (2003) found no evolution in $\Omega_{\rm C\ IV}$, the integrated contribution of C IV gas to closure density, between $z = 1.8$ and $z = 5$. The latter result is particularly surprising since $\Omega_{\rm C\ IV}$ depends on both the overall carbon abundance and the C IV ionization fraction $n_{\rm C\ IV}/n_{\rm C}$. Naively one would expect both of these quantities to vary over such a broad redshift range, because of ongoing chemical enrichment and the evolution of the ionizing background radiation spectrum.

Despite the discovery of several $z \gtrsim 6$ QSOs in the last few years (Fan et al. 2001, 2003, 2004, 2006), intergalactic absorption-line studies have been limited to $z \lesssim 5$ because at higher redshift the C IV doublet moves into the near-infrared. Absorption line spectroscopy is much more challenging in this regime because of increased detector noise, OH emission from the sky, and more severe telluric absorption. These foreground problems can be mitigated by employing higher spectral resolution, but the associated penalties in sensitivity require long integrations to overcome.

In this paper I present J band GNIRS spectra of two $z \sim 6$ QSOs at moderately high spectral resolution ($\Delta v = 60$ km/s). These spectra are searched for C IV absorption systems at $5.4 \lesssim z \lesssim 6.2$, and the results used to extend existing measurements of $\Omega_{\rm C\ IV}$ to $z \sim 6$. In section 2, I describe the observations and reduction methods. Section 3 details the C IV search procedure and simulations to quantify the effects of incompleteness and/or spurious C IV detections in the data. Sections 4 and 5 present the results for $\Omega_{\rm C\ IV}$ and a discussion of

[1] Based on observations obtained at the Gemini Observatory, which is operated by the Association of Universities for Research in Astronomy, Inc., under a cooperative agreement with the NSF on behalf of the Gemini partnership: the National Science Foundation (United States), the Particle Physics and Astronomy Research Council (United Kingdom), the National Research Council (Canada), CONICYT (Chile), the Australian Research Council (Australia), CNPq (Brazil) and CONICET (Argentina)

[2] MIT Center for Space Research, 77 Massachusetts Ave. #37-673, Cambridge, MA 02139, USA; simcoe@mit.edu
[3] Pappalardo Fellow in Physics

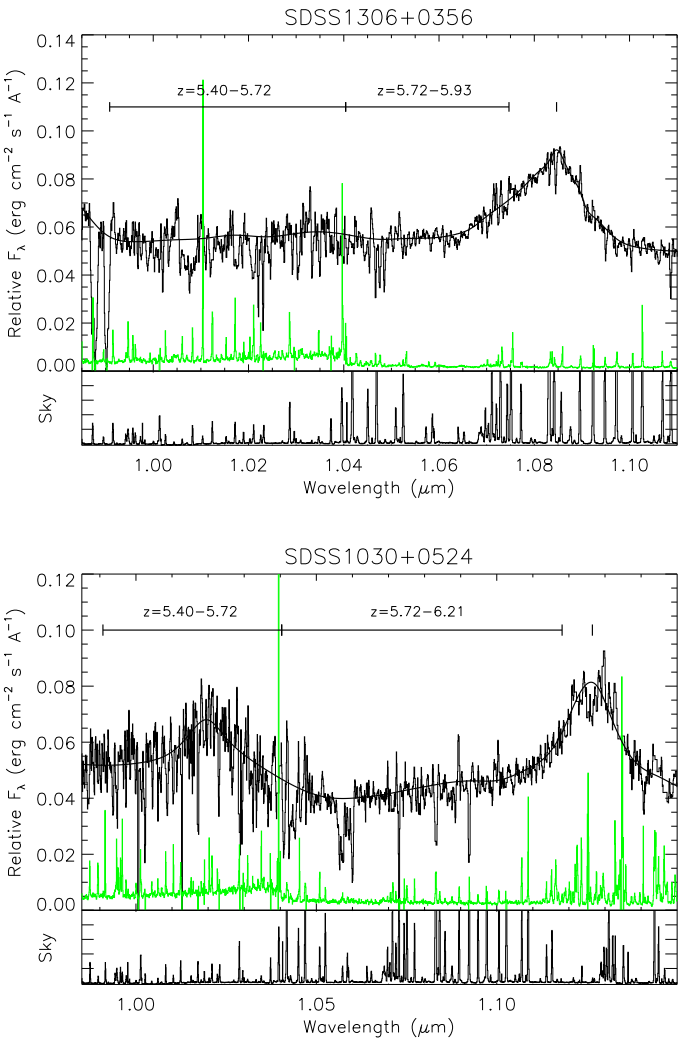

FIG. 1.— C IV spectra of $z \sim 6$ QSOs SDSS1306+0356 ($z_{em} = 6.002$) and SDSS1030+0524 ($z_{em} = 6.272$). Solid line shows continuum estimate, and light green line shows 1σ error estimates, including the effects of Poisson noise from sky emission and telluric absorption. Night Sky emission is shown in bottom panels, and the C IV search ranges are indicated with labeled horizontal bars. The redshift of the C IV emission peak is shown with a vertical dash.

their implications and limitations.

2. OBSERVATIONS

Figure 1 displays the C IV spectral regions for the high redshift QSOs SDSS1306+0356 ($z_{\rm em} = 6.002$ as measured from the C IV emission peak) and SDSS1030+0524 ($z_{\rm em} = 6.272$). The data were obtained with the GNIRS instrument (Elias et al. 1998), operated in queue mode on Gemini-South during semesters 2005A and 2006A. The instrument was configured with the cross-dispersion prism, the 110 line/mm grating, and a 0.45 arcsecond slit. Two grating positions were observed for each QSO to provide complete spectral coverage up to the emission wavelength of C IV , although the signal-to-noise ratio (SNR) is not completely uniform between setups due to varying conditions on different nights within the queue. Each QSO was observed for approximately 8 hours per setup.

The observations were split into sequences of 4×10 minute integrations, nodded four arcseconds along the slit in an ABBA configuration. The data were reduced using customized IDL software developed by the author. Individual frames were filtered for detector pattern noise and flatfielded, and the ABBA frames were combined to remove signatures of the sky, dark current, and charge persistence. Each 2D pixel was assigned a wavelength by fitting a second order polynomial to the centroids of OH sky lines, which were compared with the line lists compiled by Rousselot et al. (2000). Residual errors in the sky subtraction were corrected by a second-pass fit of a b-spline function to the subsampled grid of wavelength versus pixel intensity. Objects were identified and extracted using an optimal Gaussian profile, with errors determined by direct calculation of the sky RMS outside of the object profile (the errors were not dominated by shot noise from the object). The data were flux calibrated and corrected for telluric absorption using observations of standard stars obtained throughout the night at similar airmass as the QSOs. Finally, the extracted spectra were scaled to match in flux, and added together on a 1D grid of pixels with constant velocity spacing of 25.3 km/s. Exposures from different nights were weighted according to their $(\rm SNR)^2$, and the wavelengths converted to vacuum heliocentric coordinates. The final resolution of the combined spectra was measured as $R = 5000$ or 60 km/s FWHM (2.35 pixels) using Gaussian fits of sky lines in both the reduced 1D and the raw 2D frames.

3. ANALYSIS

The data in Figure 1 are among the first $z > 5$ IR QSO spectra with resolution suitable for absorption line measurements; however, they are still a factor of ~ 10 coarser than high resolution optical spectra at $z \sim 3$ and have lower SNR by a factor of several. At $\Delta v = 60$ km/s per resolution element, they are sufficient to resolve the C IV doublet (with characteristic $\Delta v \sim 500$ km/s). However, individual C IV components at lower redshift have typical intrinsic velocity dispersions of $b \sim 10$ km/s (Rauch et al. 1996), and hence will generally not be resolved in these spectra. Since the line broadening is dominated by instrumental effects, I have characterized the absorption systems through a curve-of-growth analysis with attention to possible saturation effects, rather than by direct Voigt profile fitting. However, all of the results were compared against Voigt profiles generated using independent software as a final consistency check.

The data were divided into two separate redshift intervals for the analysis, with the interval boundaries determined by the SNR of the data. The redshift ranges are indicated in Figure 1 by horizontal bars. In both objects an increase in the pixel noise level is seen at the transition between two spectral orders at $\lambda \approx 1.04$ μm. This established the lower boundary of the high-redshift bin at $z = 5.72$. The upper boundary of the high-redshift bin was set at $z = 6.21$, or 2500 km s^{-1} below the emission redshift of SDSS1030+0524. It is common practice in absorption line surveys to omit this last portion of spectral coverage because any absorbers there would be affected by local radiation from the QSO. For this same reason the sarch range of SDSS1306+0356 was limited to $z = 5.72 - 5.93$ for the high redshift bin. Neither SDSS1030+0524 or SDSS1306+0356 contains any C IV lines within 2500 km s^{-1} of its emission redshift, so

the results are not sensitive to this choice. Inclusion of the extra spectrum would amount to a $\sim 15\%$ (0.06 dex) increase in pathlength.

Because of its lower emission redshift, SDSS1306 does not cover the entire range of the high redshift bin. Hence the effective (pathlength weighted) central redshift of the bin falls at $z = 5.92$, slightly below the nominal midpoint of $z = 5.97$. The low redshift bin ranges from $z = 5.40 - 5.72$, with its lower bound chosen to avoid contamination from interloping Mg II at $\lambda \approx 9900\mathring{A}$ in SDSS1306+0356. Both objects cover its full width.

Because of the IR data's lower spectral resolution, lower SNR, and shorter pathlength relative to $z \sim 3$ optical surveys, this initial abundance measurement at $z \sim 6$ will not be sensitive to weak C IV systems in the very tenuous IGM. However, the data quality is high enough to detect the stronger C IV systems commonly seen in lower redshift data with high confidence. Because the slope of the C IV column density distribution is flatter than $N_{\rm C\ IV}^{-2}$ (Songaila 2001), it is these systems which provide the dominant contribution to $\Omega_{\rm C\ IV}$ (Pettini et al. 2003; Simcoe et al. 2006), and this is the main measurement presented in Section 4.2.

3.1. *Identification and Measurement of* C IV *Lines*

Each of the QSO spectra was searched systematically for C IV doublets using an automated software routine. First, an estimate of the continuum was constructed by interpolating an interactively fit cubic spline. The minimum spacing of the spline knots was set at 500 km s^{-1} to avoid overfitting the continuum on smaller scales.

The entire redshift range was then scanned for absorption feaures with $\geq 3\sigma$ significance in equivalent width (EW) over a resolution element. Each flagged feature was considered a possible 1548.2Å component of the C IV doublet, and the EW was then calculated for the corresponding 1550.8Å region. If the 1550.8Å EW was also $\geq 2\sigma$, the system was flagged as a candidate C IV doublet. The list of candidate doublets was then examined by hand to discard systems that were obviously contaminated by sky subtraction residuals or noise, or which had doublet ratios inconsistent with C IV (i.e. $W_{1551} > W_{1548}$).

Application of this procedure resulted in nine C IV detections between the two sightlines, ranging from $z = 5.451$ to $z = 6.175$. For each of these systems, I estimated a more accurate rest EW of C IV ($W_{\rm r,C\ IV}$) by fitting a Gaussian absorption profile to the data, with its width fixed at one resolution element. Plots of each system and its best-fit absorption profile are shown in Figures 2 through 4, with absorption line redshifts and EWs listed in Tables 1 and 2.

Some of the high redshift C IV lines are highly significant detections, while some are more marginal. Along the SDSS1306 sightline (which has a higher SNR) only three systems are present. The system at $z = 5.674$ is a strong detection, although it is blended with noise features in the data. The systems at $z = 5.451$ and $z = 5.927$ are much weaker and even with a high SNR over these portions of the spectrum, the C IV 1550.8Å detection significance is low.

Toward SDSS1030+0524 the search algorithm identified six C IV systems. Two strong detections are found at $z = 5.738 \pm 0.005$ and $z = 5.827 \pm 0.005$. The system at $z = 5.738$ contains two significant components, with the 1548.2Å component of one line blended with the 1550.8Å component of the other. It is found in a noisy region of the spectrum, where systematic errors in the sky subtraction are non-negligible. The $z = 5.827$ system contains three highly significant doublets. This complex also contains another strong line to the red which could

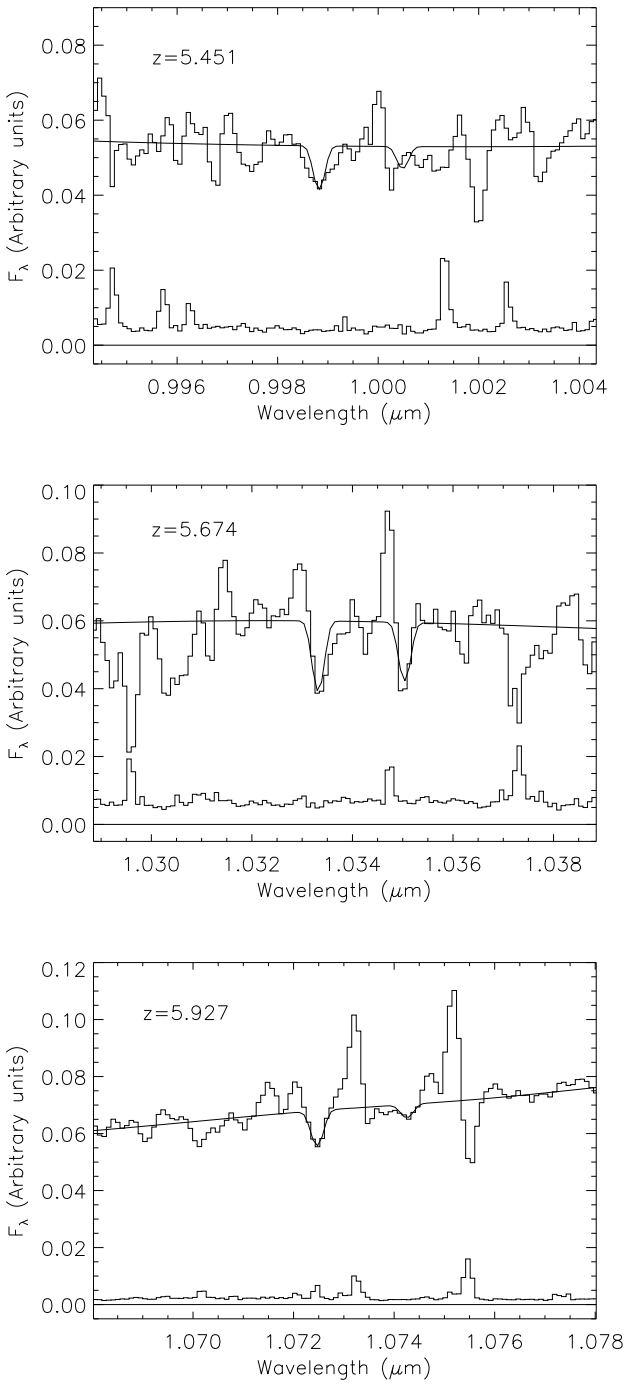

FIG. 2.— C IV detections along the line of sight towards SDSS1306+0356. Best-fit absorption models are shown with solid lines. The upper two systems are contained in the low-redshift sample; the bottom system is a marginal detection, and it is the only C IV line identified at high redshift toward this QSO.

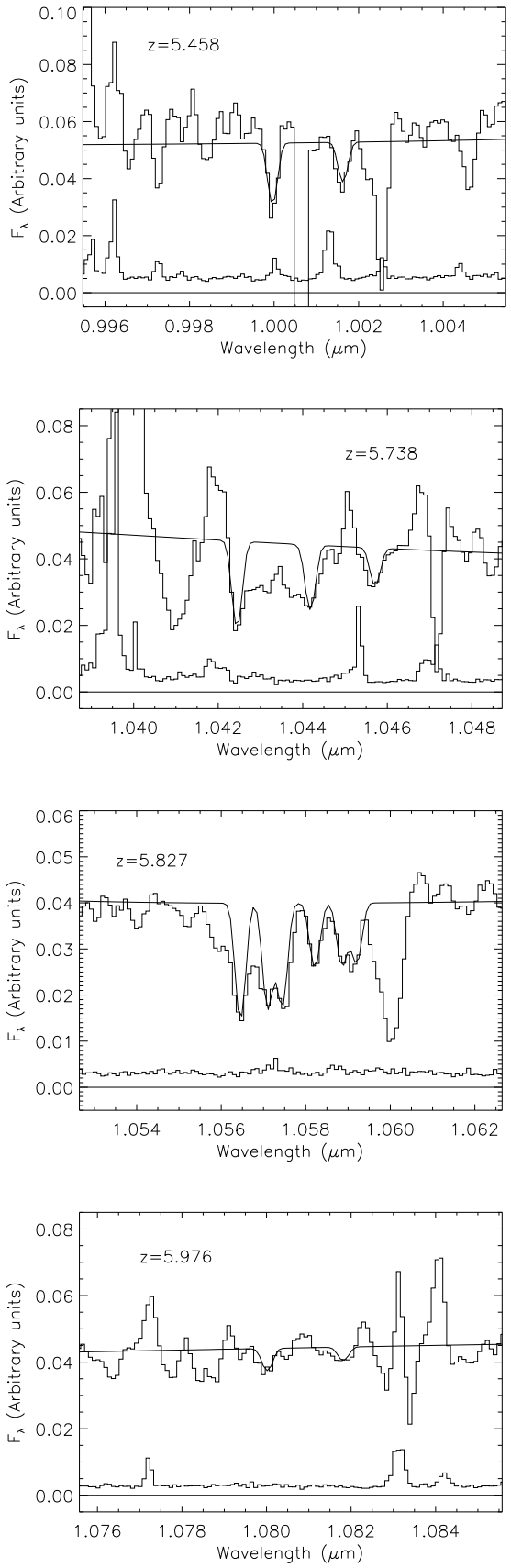

FIG. 3.— C IV detections along the line of sight towards SDSS1030+0526. Top system at $z = 5.458$ is in the low redshift sample, all others are in the high redshift sample. Best-fit absorption models are shown with solid lines.

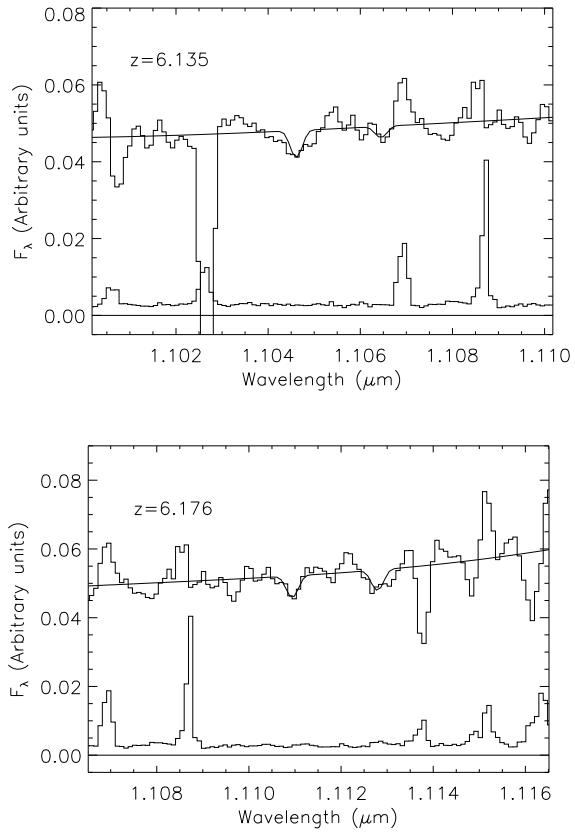

FIG. 4.— C IV detections along the line of sight towards SDSS1030+0526 (Continued from previous figure).

not be identified with any ion commonly seen in QSO spectra at any redshift. All well-known QSO lines with rest wavelengths between 1450Å (corresponding to the QSO's rest frame) and 6000Å (i.e. past the NaD doublet) were considered without finding a match. The presence of this absorption was verified in the 2D trace over multiple nights, and checked to rule out artifacts from telluric absorption or features in the flat field. It was also checked against a high-resolution optical spectrum of SDSS1030 (kindly provided by G. Becker) without resulting in any cross-identification. The most likely interpretation appears to be a mixture of three C IV components with one additional unidentified line.

Only two weak C IV systems are identified at $z > 6$. They are each near the detection limit of the data, and both are found in relatively clean and sky-free portions of the spectra. It is intriguing that the strong C IV systems generally seem to be found at $z \lesssim 5.9$, while at $z \gtrsim 5.9$ (where the SNR of our data is highest) the C IV systems are weaker. While this could be consistent with some evolution of the population, this effect could also be caused by shot noise along a short redshift path, as described in more detail in Section 4.1.

Some, but not all, of the C IV doublets show evidence of instrumentally unresolved saturation in the physical absorption profile. Figure 5 shows the C IV curve-of-growth (COG) of rest EW (W_r) versus $N_{\rm C\,IV}$; the bottom panel displays the EW ratio between the two components as a

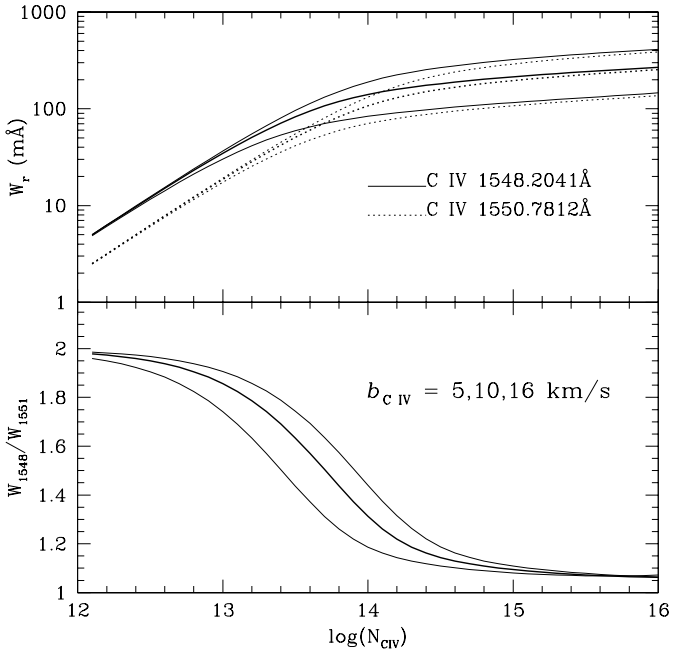

FIG. 5.— Curve-of-growth calculations for C IV . Top panel shows the relation of W_r to $N_{\rm C\ IV}$ for both components of the doublet. Bottom panels shows the equivalent width ratio of the two doublet components as a function of $N_{\rm C\ IV}$, for three typcal choices of b parameter.

function of $N_{\rm C\ IV}$ for various values of the C IV b parameter. For reasonable values of $b_{\rm C\ IV}$, the 1548.2Å component begins to saturate near $N_{\rm C\ IV} \sim 10^{13}$ cm^{-2}, and the doublet ratio approaches unity as the 1550.8Å component also begins to saturate at $N_{\rm C\ IV} \sim 10^{14}$ cm^{-2}.

Column 7 in Tables 1 and 2 shows the measured doublet ratio for each C IV detection. Because of the data's sensitivity limitations, most of the detected systems lie in the non-linear regime between $10^{13} \lesssim N_{\rm C\ IV} \lesssim 10^{14}$ cm^{-2}, where the $N_{\rm C\ IV} - W_r$ mapping is degenerate with the C IV b parameter. However, even for some of the stronger systems in the data with $W_r \sim 200 - 300$ mÅ (e.g. the complex at $z = 5.823 - 5.830$), the doublet ratios provide useful upper bounds on $N_{\rm C\ IV}$. Often the ratio is larger than one would guess from measuring $W_r(1548)$ alone, and in these cases it is likely that the observed C IV line is actually an unresolved blend of several narrow components with more complex velocity structure.

At $z \sim 3$, the typical C IV line has a velocity dispersion of $b \approx 10$ km s^{-1}, and over 80% of C IV components have $b_{\rm C\ IV} \leq 16$ km s^{-1}(Rauch et al. 1996). Assuming $b_{\rm C\ IV} = 10$ km s^{-1} for our systems, the doublet ratio can be used to estimate $N_{\rm C\ IV}$. Then, the number of unresolved components can be inferred by comparing the measured value of W_r with the single-component value from the COG. The rightmost columns in Tables 1 and 2 show the $N_{\rm C\ IV}$ value deduced from the EW ratios, along with the corresponding number of components required to match the total EW for each system.

The $N_{\rm C\ IV}$ values for individual components range between $10^{13.15}$ and $10^{14.3}$. Different choices of $b_{\rm C\ IV}$ can change specific values of $N_{\rm C\ IV}$ by up to ~ 0.2 dex; random measurement errors in the EW could add another 0.2 dex of uncertainty, though these errors would be uncorrelated. However, the *total* column density of each C IV system is fairly insensitive to the specific choice of b. A larger b parameter leads to fewer unresolved components with higher $N_{\rm C\ IV}$, while a small b leads to more components with smaller column densities, but the sum of the columns matches to within < 0.1 dex for any choice of b between 5 and 20 km s^{-1}.

3.2. *Estimates of Sample Completeness*

IR absorption line searches require particular attention to characterize sample incompleteness and false-positive identifications. In addition to normal SNR variations in the data, one encounters many spectral regions where Poisson noise from OH sky emission or residuals from imperfect telluric absorption correction render pixels unusable for cosmological absorption measurements. At $R = 5000$, the GNIRS spectra resolve sky features well enough to work in many of the dark regions between fetures from the night sky.

To quantify the completeness of the $z \sim 6$ C IV sample as a function of $N_{\rm C\ IV}$, we have performed a series of Monte Carlo simulations. For each redshift bin in each sightline, a sample of artifical C IV doublets was created with $N_{\rm C\ IV}$ ranging from $10^{12} - 10^{16}$ cm^{-2} and redshifts selected at random. Each artifical line was added individually into the real spectrum, and the data were searched using the same EW criteria to see if the artificial line was recovered. One thousand trials were performed for each column density.

Figure 6 displays $f_{\rm comp}$, the fraction of lines recovered as a function of $N_{\rm C\ IV}$ for each of the sightlines. For most of the redshift path, the data are largely complete ($\gtrsim 70\%$) at $N_{\rm C\ IV} \gtrsim 10^{14}$ cm^{-2}. The completeness drops off rapidly towards $N_{\rm C\ IV} \leq 10^{13}$ cm^{-2}, at which point only $5 - 10\%$ of systems are detected. In the IR, unlike the optical, it is nearly impossible to achieve 100% completeness even at thie highest column densities because of chance coincidences with OH sky lines or strong telluric features. However, for the C IV lines at $N_{\rm C\ IV} \gtrsim 10^{14}$cm^{-2}, it appears that at $R \sim 5000$ one resolves night sky foregrounds out of $\sim 80\%$ of the total available pathlength.

Sample incompleteness effectively reduces the absorption pathlength over which lines of a given column density can be detected in the survey. In the discussion below, we explicity state when completeness corrections are applied to the data. These are implemented by scaling the relevant pathlengths ΔX by the factors shown in Figure 6.

3.3. *Incidence of False Positive Identifications*

Several of the C IV detections in Tables 1 and 2 approach the sensitivity limit of the data, and at these column densities one must also consider the possibility of false positive identifications from chance noise fluctuations. This process is much more difficult to simulate since in true spectra the noise properties are often not perfectly approximated by a Poisson distribution, especially in the very instances where correlated pixels lead to false detections.

One method for quantifying the false positive rate is to scan the spectra for absorption "doublets" identical to

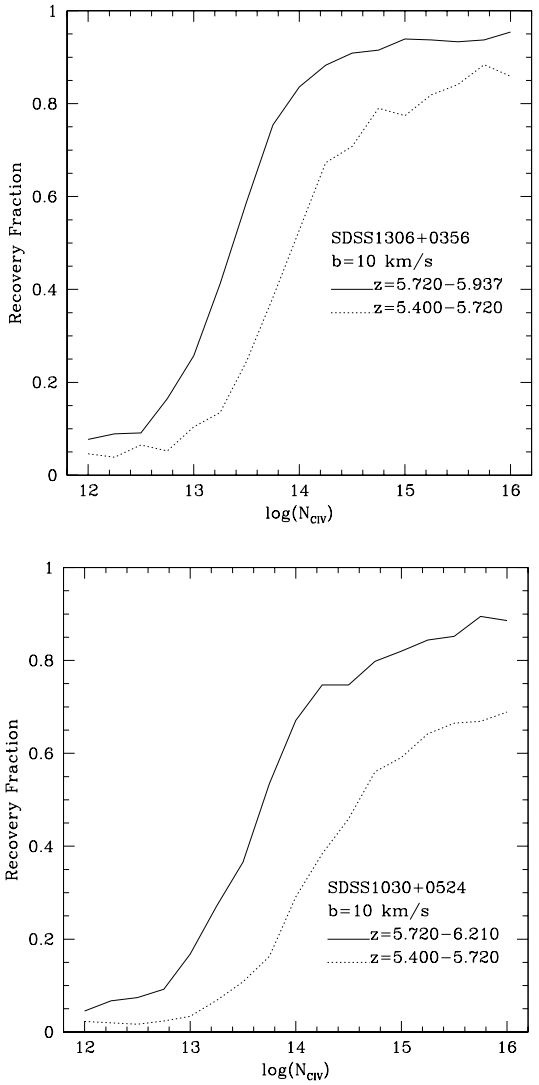

FIG. 6.— Estimates of sample completeness as a function of $N_{\rm C\ IV}$, determined from Monte Carlo simulations performed on the data. Top panel shows completeness for SDSS1306 over both sample redshift bins; bottom panel shows the same for SDSS1030. C IV lines are recovered more completely in the higher redshift bins because of improved SNR in these spectral regions.

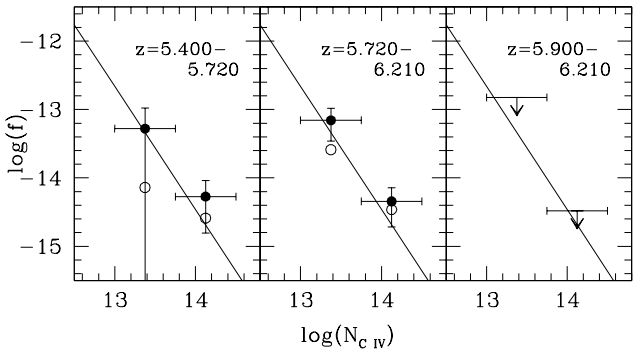

FIG. 7.— The C IV column density distribution function, defined as $f(N_{\rm C\ IV}) = d\mathcal{N}/dN_{\rm C\ IV}dX$, over three different redshift intervals. Points are shown with incompleteness corrections; the uncorrected values are shown with open circles. Left and center panels show the measured CDDF for the nominally defined redshift bins. The right panel illustrates limits for a possible high redshift bin, where more absorption pathlength would be required to obtain an accurate measurement.

C IV in every sense, except that the oscillator strengths of the two transitions are reversed. Systems identified this way will be subject to the same noise properties and line spacing as true C IV, but can only be caused by correlated noise fluctuations in the data since a doublet with $W_r(1551) > W_r(1548)$ is unphysical.

I searched for this type of system in the two QSO spectra using the same EW criteria as for the true C IV search. For SDSS1306, the high redshift sample at $z = 5.72-5.93$ yielded one weak "false" system. For SDSS1030, there was one (rather strong) flase system at $z = 5.722$, and two other weak systems at $z = 6.005$ and 6.155. Over the full $z = 5.72 - 6.21$ redshift path, the total column density of all "true" C IV systems is $10^{14.8}$ cm^{-2}, whereas the the total for the "false" systems was $10^{14.3}$ cm^{-2}. Contamination from false positives may therefore comprise up to $\lesssim 30\%$ of the reported C IV in this bin, but spurious detections do not appear to dominate over the true C IV signal. In the $z = 5.40 - 5.72$ bin the false positive signal is likewise estimated at $\lesssim 25\%$.

If one restricts the search to the $z \gtrsim 6$ region, the contribution from contaminants is no longer subdominant. The integrated C IV column for the three "true" C IV systems is $\sum N_{\rm C\ IV} = 10^{13.6}$ cm^{-2}, whereas the two "false" systems have $\sum N_{\rm C\ IV} = 10^{13.7}$. This result is consistent with the interpretation that *all* of our $z > 6$ C IV detections are spurious, or alternatively that there is no statistically significant signal from C IV over $z = 6.0 - 6.21$ in SDSS1030. This is an intriguing possibility, but the absorption pathlength is fairly short for this one sightline, so it could just be the result of statistical fluctuations in a small sample. I return to this point in the discussion; for the purpose of calculations below I continue to treat the $z > 6$ C IV detections as real, keeping in mind that because of contamination they will lead to upper limits on the values of any derived quantities.

4. RESULTS

4.1. $z \sim 6$ C IV *Column Density Distribution*

A key result from lower redshift C IV surveys (e.g. Songaila 2001) is that the column density distribution function (CDDF) of C IV —defined as the number of absorbers per unit $N_{\rm C\ IV}$ per unit absorption pathlength—is nearly invariant between $z \sim 2$ and $z \sim 5$. Even with the small sample available at $z \sim 6$, one can construct a coarse CDDF for comparison with this lower redshift data.

For calculating the absorption pathlength, I use the convention that $\Delta X = X(z_2) - X(z_1)$, where $X(z)$ is defined as

$$X(z) = \frac{2}{3\Omega_M}\sqrt{\Omega_M(1+z)^3 + \Omega_\Lambda} \qquad (1)$$

with $\Omega_M = 0.3$ and $\Omega_\Lambda = 0.7$. Results from the literature are often quoted using the ΔX for an Einstein-deSitter universe; where appropriate I have rescaled the literature values by $\sqrt{\Omega_M}$ to conform with more recent concordance models.

Given the small size of the $z \sim 6$ line sample, I only estimate the CDDF in two $N_{\rm C\ IV}$ bins—one ranging from $\log(N_{\rm C\ IV}) = 13.00 - 13.75$ and one from $\log(N_{\rm C\ IV}) = 13.75 - 14.5$. For consistency, I have followed the approach of Songaila (2001), summing the $N_{\rm C\ IV}$ values of individual components in each C IV complex to obtain a single, total column density for the system. For example, the lines spanning $z = 5.82374 - 5.83012$ were treated as a single system with $N_{\rm C\ IV} = 10^{14.42}$, corresponding to the sum of the individual components listed in Table 2.

The resulting distributions are shown in Figure 7 and Table 3. The solid line shows the fit to the C IV CDDF derived from the $z \sim 3$ sample of Songaila (2001), after rescaling to $\Omega_M = 0.3$. The open circles indicate the $z \sim 6$ CDDF values obtained before correcting for sample incompleteness (as described in Section 3.2). Completeness corrected points are shown with solid dots; the corrections were made by rescaling ΔX by the recovery fractions shown in Figure 6. The horizontal error bars indicate bin sizes, and the vertical bars indicate Poisson counting errors.

Despite the modest size of the $z \sim 6$ sample, the data do appear to be consistent with a non-evolving form of the CDDF at $z = 5 - 6$. In the primary sample with highest data quality at $z = 5.72 - 6.21$, the data fall directly on top of the low redshift fit. In the lower redshift bin the SNR is also lower so the sample is substantially incomplete (e.g. there is only one system in the the low column density bin, and we expect sample contamination). However, within substantial errors even this sample is consistent with a non-evolving distribution.

It would be stretching the data somewhat to consider these calculations a detailed measurement of the CDDF at $z \sim 6$; a full and accurate measurement would require both more sightlines to build up ΔX at $N_{\rm C\ IV} \gtrsim 10^{14}$ cm^{-2} (where our sample is mostly complete), and higher SNR data to improve the sample completeness for weaker lines at $N_{\rm C\ IV} \lesssim 10^{13.5}$ cm^{-2}. However, the fact that we detect any lines at all argues against a strong downward trend in the C IV abundance between redshift 5 and 6, and the similar overall normalization (about one system per unit absorption path, per logarithmic unit column density) suggests that these is no statistically significant evidence for evolution.

It is notable that within the $z = 5.72 - 6.21$ bin, most of the C IV absorption is concentrated at the bluest end; in fact in Section 3.3 it was suggested that for $z \gtrsim 5.9$ the data may be statistically consistent with no C IV signal. It is tempting to interpret this as a hint of decline in the C IV abundance, but there are dangers in this sort of *a posteriori* definition of a redshift boundary, particularly for small sample sizes (recall that the redshift bins for the main sample were bounded only by random factors: a change in the noise properties of the data, and the QSO emission redshifts).

Nevertheless, for argument's sake one can ask whether the lack of C IV at $z \gtrsim 5.9$ should be surprising given the amount of absorption path covered in the SDSS1030+0526 spectrum. In the rightmost panel of Figure 7, we separate out the $z = 5.9 - 6.28$ redshift range, and indicate the upper limits derived from assuming that there is < 1 system at $\log(N_{\rm C\ IV}) = 13.75 - 14.50$ (we detected none) and ≤ 4 systems at $\log(N_{\rm C\ IV}) = 13.0 - 13.75$ (we detected 4 systems, but also 3 false positives). Taking just the strong systems at $N_{\rm C\ IV} = 10^{13.75-14.5}$ which should be easily detected, the completeness-corrected absorption pathlength in the SDSS1030 sightline is only marginally large enough ($\Delta X = 1.16$) to expect a single strong C IV detection, so the absence of strong C IV could be the result of a statistical fluctuation. The probability of observing zero strong systems in SDSS1030 at $z \gtrsim 5.9$ can be estimated from $f(N_{\rm C\ IV})$ (the C IV CDDF) as:

$$P(0) = \exp\left[-f(N_{\rm C\ IV})\Delta X \Delta N_{\rm C\ IV}\right] \approx 50\%. \qquad (2)$$

So, for the present, the possibility of a decline in C IV abundances at $z \gtrsim 5.9$ remains intruiging but the sample is too small to make conclusive statements. If the CDDF remains constant at $z \gtrsim 6$, then there is a $\sim 75\%$ chance that a strong system will be detected in the next sightline to be searched at $z \geq 6$.

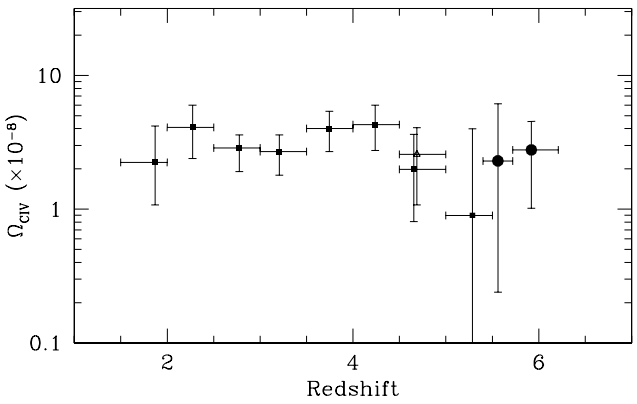

FIG. 8.— Evolution of the C IV contribution to closure density. New points are shown with round dots at $z = 5.40 - 5.72$ and $z = 5.72 - 6.21$. Verical error bars represent 90% confidence intervals. Results at $z = 1.8 - 5.5$ from Songaila (2001) are shown with squares, and the $z = 4.5 - 5.0$ point from Pettini et al. (2003) is shown with an open triangle. All values are scaled to $h = 0.71$, $\Omega_M = 0.3$, and $\Omega_\Lambda = 0.7$.

4.2. $\Omega_{\rm C\ IV}$: *Contribution to Closure Density*

The integral of the CDDF (weighted by $N_{\rm C\ IV}$) can be used to estimate the volume-averaged density of C IV atoms over a specified redshift interval. This quantity is customarily normalized by the critical density ρ_c to yield $\Omega_{\rm C\ IV}$, which is calculated from observed quantities as:

$$\Omega_{\rm C\ IV} = \frac{1}{\rho_c} m_{\rm C\ IV} \frac{\sum N_{\rm C\ IV}}{\frac{c}{H_0}\sum \Delta X} \qquad (3)$$

where $m_{\rm C\ IV}$ is the mass of the C IV ion. This integrated C IV density provides a conveient metric for studying the redshift evolution of C IV abundances. Songaila (2001) has compiled measurements of $\Omega_{\rm C\ IV}$ in the $z = 2 - 5$ interval; Pettini et al. (2003) have also published a measurement at $z = 4.5 - 5.0$. Figure 8 displays these prior results, for $H_0 = 71$ km s^{-1}Mpc^{-1}, and ΔX rescaled as above for $\Omega_M = 0.3$ and $\Omega_\Lambda = 0.7$.

The rightmost points show the two new estimates of $\Omega_{\rm C\ IV}$ at $z = 5.40 - 5.72$ and $z = 5.72 = 6.21$ from this analysis. Horizontal error bars indicate the bin ranges,

and vertical error bars represent 90% confidence intervals calculated as in Pettini et al. (2003), using the error estimator of Storrie-Lombardi et al. (1996):

$$\frac{\Delta(\Omega_{\rm C\ IV})}{\Omega_{\rm C\ IV}}(90\%) = 1.64 \times \sqrt{\frac{\sum N^2_{\rm C\ IV}}{\left(\sum N_{\rm C\ IV}\right)^2}} \qquad (4)$$

The new points in Figure 8 have been corrected for sample incompleteness by scaling each line's column density in the sum from Equation 3 by the pathlength over which it could be detected. It is also corrected for spurious contamination by subtracting off the total column density of false-positive lines identified in each bin (see Section 3.3). These two corrections are both of order ~ 0.2 dex but act in opposite directions.

The $z \sim 6$ points follow the trend of a constant $\Omega_{\rm C\ IV}$ established at lower redshift, and do not show evidence for a decline at $z \gtrsim 5$. While some hints of a declining $\Omega_{\rm C\ IV}$ were present in the optical data at $z \sim 4.5 - 5.5$, this may be an artifact of shot noise, as was pointed out by Songaila in the work where it was reported. The $z = 5 - 5.5$ range is still particularly difficult for such measurements because of the low sensitivities of both CCDs and IR focal plane arrays at $\lambda \sim 0.98\mu$m, and the substantial atmospheric foregrounds. Both Songaila's measurement at $z = 5 - 5.5$ and the new point at $z = 5.4 - 5.72$ are limited by shot noise. A pathlength-weighted average of the two points yields $\Omega_{\rm C\ IV}(5.00 - 5.72) = 3.6^{+2.9}_{-3.5} \times 10^{-8}$, consitent with the full redshift range, though still with substantial error bars. In the present sample the $z = 5.72 - 6.21$ point is more reliable, since it incorporates more absorption path, it is situated in a cleaner portion of the Y band, and it represents data with a higher SNR. The error bars for both $z \sim 6$ points are larger than for the lower redshift data because we have only sampled two sightlines; however since redshift path is a comoving quantity proportional to $(1 + z)dz$ the effective path per sightline increases at higher reshift for $\Omega_{\rm C\ IV}$ measurements.

Given the resolution and SNR of the $z \sim 6$ spectra, even a single C IV detection is enough to bring $\Omega_{\rm C\ IV}$ up to the $\sim 10^{-8}$ level. If the C IV density was in rapid decline at $z \gtrsim 5$, no C IV lines should have been detected in the GNIRS spectra, and in this case our sensitivity would have been sufficient to set upper limits roughly a factor of 3 below the $\sim 3 \times 10^{-8}$ level seen at lower redshift. Since several C IV lines are detected, even if a fraction of these are false-positives, it seems unlikely that they could mask an order-of-magnitude decline in $\Omega_{\rm C\ IV}$ at $z \sim 6$.

5. DISCUSSION

5.1. *Implications for Cosmic Abundances*

The $z \sim 6$ C IV systems detected in SDSS1030+0524 and SDSS1306+0256 yield an $\Omega_{\rm C\ IV}$ value of $\approx 3 \times 10^{-8}$, which is essentially identical to the value observed at lower redshift. However, this measurement reflects only the C IV abundance, and does not take into account the fraction of carbon atoms in other ionization states.

A correction for ionization requires estimates of $f_{\rm C\ IV} = n_{\rm C\ IV}/n_{\rm c}$—a factor which varies with redshift and environment and can be large. In ionization equilibrium, the exact value of $f_{\rm C\ IV}$ depends upon the density ratio of ionizing photons to baryons as well as the shape of the background radiation spectrum. At high redshift, the ionizing background becomes less intense because of the declining QSO luminosity function, and softer because of an increasing contribution from galaxy light. Also, the average gas density increases as $(1 + z)^3$, leading to a decline in the overall ionization level.

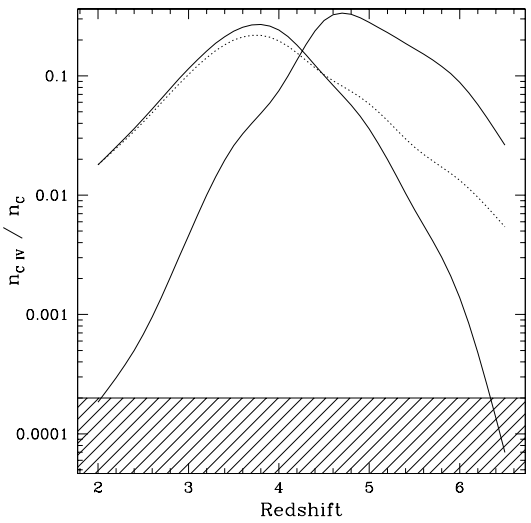

FIG. 9.— The fraction of carbon atoms in the C IV ionization state, as a function of redshift. Solid lines indicate the evolution for baryonic overdensities of $\rho/\bar{\rho} = 1$ and $\rho/\bar{\rho} = 10$, with the $\rho/\bar{\rho} = 10$ curve peaking at $z \sim 3.8$ and the $\rho/\bar{\rho} = 1$ curve peaking at $z = 4.75$. Dotted line indicates model for $\rho/\bar{\rho} = 10$, but with additional local radiation from a galaxy at a distance of 100 kpc. The hatched region is excluded on the basis that it would lead to super-solar IGM abundances.

The net effect of these changes is illustrated in Figure 9, which shows the evolution of $f_{\rm C\ IV}$ from $z \sim 2 - 6$. These calculations were performed using the CLOUDY photoionization code (Ferland et al. 1998), with a background radiation spectrum containing both QSOs ($f_\nu \propto \nu^{-1.8}$) and galaxies (with 10% escape fraction of ionizing photons) after propegation through the IGM (Haardt & Madau 2001). The spectra were normalized to be consistent with measurements of the proximity effect in QSOs (Scott et al. 2000) and the distribution of flux transmission in the Ly-α forest (McDonald & Miralda-Escudé 2001). The normalization becomes quite uncertain approaching $z \sim 6$; in this range I have estimated its value at by extrapolating from lower redshift data. The two solid lines indicate the C IV ionization fractions for gas with $\rho/\bar{\rho} = 1$ and 10, where $\bar{\rho} = \Omega_b \rho_c (1 + z)^3$. At $z \sim 2$, the intense radiation from QSOs ionizes most carbon to C V and other states higher than C IV. As one progresses through $z \sim 4$, the C IV fraction reaches its maximum and then declines rapidly at $z \gtrsim 4.5$ as the carbon becomes more neutral.

The total variation in $f_{\rm C\ IV}$ spans 2-3 orders of magnitude from $z \sim 2 - 6$ for a given overdensity. However, it approaches a maximum value of $f_{\rm C\ IV} \approx 0.3$ independent of density, though the corresponding redshift does vary with $\rho/\bar{\rho}$. As pointed out by Songaila (2001), this fact can be used to set a lower limit on the overall carbon abundance at high redshift of $\Omega_{\rm C} \gtrsim \Omega_{\rm C\ IV}/0.3 \approx 1 \times 10^{-7}$. This can be compared to the overall baryon density

$\Omega_b h^2 = 0.022$ (O'Meara et al. 2001) to obtain an volume-averaged carbon abundance:

$$\left[\frac{\mathrm{C}}{\mathrm{H}}\right] \gtrsim \log\left(\frac{\Omega_{\mathrm{C}}}{\Omega_b}\right) - \log\left(\frac{m_C}{\mu m_H}\right) - \log\left(\frac{\mathrm{C}}{\mathrm{H}}\right)_\odot \quad (5)$$
$$\approx -3.16.$$

Here, m_C and m_H represent the atomic mass of carbon and hydrogen, μ is the mean atomic mass in the IGM (assumed to be 1.3), and the last term represents the solar carbon abundance by number, assumed to be 3.3×10^{-4} (Grevesse & Sauval 1998).

It should be heavily emphasized that this value does not represent a ubiquitous metallicity floor in the IGM. Rather it is a volume average over the entire redshift pathlength, which contains small regions with strong C IV absorption, and large regions with no detectable C IV . The expectation value of $n_{\mathrm{C\ IV}}$ will be substantially lower than $\Omega_{\mathrm{C\ IV}}\rho_c(1+z)^3$ for most randomly chosen volumes, except for a few regions where it is much higher than this mean value. However, Equation 5 does provide a global average which may be appropriate for comparing against the integrated metal content, for example, within an entire cosmological simulation volume.

As a final note, it would also be interesting to measure the abundance of other carbon and/or silicon ions (e.g Si IV 1400, or C II 1334), since the ratios of these ions probe both relative heavy element abundances and the shape of the ionizing background spectrum (which is of particular interest during reionization at $z \gtrsim 6$). Unfortunately the SNR of the present data are not sufficient to significantly constrain Si IV/C IV or other ion ratios, though this will be an important goal of future observations.

5.2. *What does $\Omega_{\mathrm{C\ IV}}$ Represent?*

The distribution of C IV shows several remarkable properties that might not be expected *a priori*. The most obvious of these is the near-constant value of $\Omega_{\mathrm{C\ IV}}$ from $z = 2$ to $z = 6$. The measurements are identical to within errors—even accounting for the 90% confidence intervals shown in Figure 8, $\Omega_{\mathrm{C\ IV}}$ can vary by no more than a factor of ~ 3 over this complete redshift range. This comes despite the fact that $f_{\mathrm{C\ IV}}$ can vary by up to 3 orders of magnitude, and the expectation that cosmic abundances should decline on average towards higher z. In order to keep $\Omega_{\mathrm{C\ IV}}$ constant, the evolution in ionization would need to precisely cancel an opposite evolution in the carbon abundance, a scenario that is possible, but which requires fine-tuning.

Second, the C IV mass is distributed very unevenly. In the $z \sim 5.72 - 6.21$ bin, 43% of the C IV atoms are contained within a single system (at $z = 5.823 - 5.830$ in SDSS1030). A similar segregation of C IV mass is seen at all redshifts. This is related to the fact that the CDDF slope is shallower than $N_{\mathrm{C\ IV}}^{-2}$; so that the integral $\Omega_{\mathrm{C\ IV}} \propto \int N_{\mathrm{C\ IV}} f(N_{\mathrm{C\ IV}}) dN_{\mathrm{C\ IV}}$ is dominated by the strongest system in any sample.

At lower redshifts ($z \sim 2.5 - 3.5$), there is evidence that the strongest C IV absorption systems arise in the outer halos of star forming galaxies (Simcoe et al. 2006; Adelberger et al. 2003). They are often accompanied by heavy element absorption from many other ions including O VI , and their physical characteristics suggest a relation to energetic feedback from galaxy formation. Absorption from feedback-related systems comprises at least half of the $\Omega_{\mathrm{C\ IV}}$ integral at $z \sim 3$ (Simcoe et al. 2006; Songaila 2006), and these lower redshift systems share some features with the $z \sim 6$ C IV systems. In particular the range of C IV column densities and complexity of velocity structure seem to be similar for the strongest C IV systems at all epochs.

This may provide one natural explanation for the constant value of $\Omega_{\mathrm{C\ IV}}$ with redshift. If the C IV traced by the strong systems is produced locally by star forming galaxies, they can be enriched to $0.01 - 0.1 Z_\odot$ levels on short timescales. In this case, $\Omega_{\mathrm{C\ IV}}$ would be related more closely to the instantaneous metal production (i.e. star formation) rate at a given redshift, rather than the cumulative stellar mass formed prior to the epoch of observation. Much like $\Omega_{\mathrm{C\ IV}}$, the star formation rate density appears to evolve fairly little between $z = 2 - 6$ (e.g. Giavalisco et al. 2004; Steidel et al. 1999; Thompson et al. 2006). Furthermore, if the C IV absorbers reside near forming galaxies then the spectrum of ionizing radiation that they see would be augmented by local starlight, providing a buffer against large variations in $f_{\mathrm{C\ IV}}$.

In Figure 9, I illustrate this effect in the dotted curve, which shows the evolution of $f_{\mathrm{C\ IV}}$ for the same Haardt & Madau diffuse background spectrum, but with an additional star forming galaxy located 100 kpc from the absorption system. The galaxy template spectrum is taken from the Starburst99 archive (Leitherer et al. 1999). It has a stellar age of 300 Myr, and has been reddened using a Calzetti et al. (1994) extinction law with $E(B-V) = 0.155$ (Shapley et al. 2001). The total stellar mass is $10^8 M_\odot$.

The galaxy has little effect on the ionization balance at $z \lesssim 4.5$, but at higher redshift the added galaxy flux does begin to contribute such that $f_{\mathrm{C\ IV}}$ drops by only an order of magnitude from its peak, rather than $2-3$ orders of magnitude as it would otherwise have done. It seems plausible that a decline in $f_{\mathrm{C\ IV}}$ of a factor of $\lesssim 10$ could be coupled with a factor of $\lesssim 10$ decline in the carbon abundance at high redshift, resulting in weak observed evolution in $\Omega_{\mathrm{C\ IV}}$.

The other possible scenario invokes a balance of several effects to produce a flat $\Omega_{\mathrm{C\ IV}}(z)$, and does not require a local origin for the observed C IV absorbers. In this interpretation, the C IV systems trace intergalactic regions of increasingly smaller overdensity at higher redshift, in essence picking out the density where the C IV ionization fraction (or $f_{\mathrm{C\ IV}}$ times the heavy element abundance) peaks at any particular redshift. One can infer from a comparison of the solid lines in Figure 9 that this provides an independent mechanism to suppress the variation in ionization parameter with redshift. It would require a fairly uniform distribution of carbon abundance across all densities of gas in the IGM, which although more difficult to achieve at high redshift, may still be possible.

This explanation is difficult to test observationally, since at high redshift one also loses information about the local density field (because of saturation and blending within the H I Lyman alpha forest). Naively one would expect $d\mathcal{N}/dX$ for C IV to increase with redshift in this scenario (an effect which is not observed), un-

less the actual chemical abundances correlate with IGM density in just the right fashion.

This "balancing" hypothesis convolves the evolution of several competing factors (characteristic densities, ionization parameters, and chemical enrichment), so its ultimate evaluation will be best accomplished through "observations" of numerical simulations which incorporate models of chemical feedback. Indeed, Oppenheimer & Davé (2006) have very recently run simulations where galactic wind prescriptions motivated by local observations seem to strike the balance required to match the $z = 2 - 5$ observations. In their simulations there is evidence that $\Omega_{\rm C\ IV}$ should start to turn down by $z \sim 6$ in contrast to the findings presented here. However, the level of this discrepancy is probably not alarming when one takes into account both our measurement uncertainties and uncertainties in the contribution from unresolved small-scale C IV structures in the simulations.

6. CONCLUSIONS

This paper presents moderate resolution spectra of two $z \sim 6$ QSOs, taken with GNIRS on Gemini South. These spectra were systematically searched for high redshift intergalactic C IV absorption, using objective selection criteria. Comprehensive testing was performed to quantify the C IV sample incompleteness as a function of $N_{\rm C\ IV}$, as well as the rate of false positive C IV identifications. Over the primary redshift range of $z = 5.72 - 6.21$, the sample is largely complete at $N_{\rm C\ IV} \sim 10^{14}{\rm cm}^{-2}$, and drops uniformly to about $5 - 10\%$ at $N_{\rm C\ IV} \sim 10^{13}$; at lower redshift the completeness is somewhat worse because the data have a lower SNR. However, this sensitivity is adequate to construct a rough estimate of the C IV column density distribution $f(N_{\rm C\ IV})$, and also to measure the integrated density $\Omega_{\rm C\ IV}$ at a level two to three times below the observed value at $z = 2 - 5$. The main results are as follows:

1. Nine C IV absorption lines are identified between $z = 5.72$ and $z = 6.21$. Three of the these lines are contained within a single strong complex at $z = 5.827 \pm 0.004$ toward SDSS1030+0524. This single system contains 43% of the C IV atoms along the total combined redshift path. Three additional C IV lines are detected in a lower redshift bin ranging from $z = 5.40 - 5.72$. After adjusting for absorption pathlength and incompleteness, the density of lines is similar in both redshift bins.

2. The spectral region at $z \geq 6$ in SDSS1030+0524 is statistically consistent with a complete lack of C IV absorption. However, with only one sightline sampled at present this could easily be the result of a statistical fluctuation.

3. A coarse-binned representation of the $z \sim 6$ C IV column density distribution is consistent with the redshift-invariant form reported over the $z = 2 - 5$ range by Songaila (2001).

4. An extension of the $\Omega_{\rm C\ IV}(z)$ plot to $z \sim 6$ does not show evidence of a downturn in the integrated C IV abundance, at least within the factor of ~ 3 allowed by measurement errors.

Over such a large redshift range, it is remarkable to derive a constant form for the C IV column density distribution and also for $\Omega_{\rm C\ IV}$. The baryonic density, ionizing background spectrum, and metallicity should all evolve substantially between $z = 2 - 6$, so it would represent an interesting coincidence if these effects all cancelled. In principle it is possible to mask the effect of evolution in the C IV ionization fraction if the C IV absorbers are associated with regions of lower overdensity at higher redshifts. In this case one might anticipate an increase in $d\mathcal{N}/dX$ at higher z, but this is not observed. Because of the complex interplay of many evolving factors, a full evaluation of this explanation for the constancy of $\Omega_{\rm C\ IV}$ with z requires comparison with numerical simulations (e.g. Oppenheimer & Davé 2006).

An attractive alternative explanation is that the $\Omega_{\rm C\ IV}$ measurements are dominated by strong absorbers whose properties are affected by local chemical and radiative feedback from nearby galaxies. This association appears to be present at $z \sim 2.5$, where luminous galaxies are seen directly in the neighborhood of many/most strong C IV systems. Although the same galaxies cannot be seen at high redshift, they would in principle provide a mechanism to rapidly enrich the C IV absorbing regions, and their radiation would also regulate the ionization balance of the carbon, preventing it from becoming too neutral for detection in C IV .

Local feedback models become more compelling at the highest redshifts, where the elapsed time betewen the onset of reionization ($z \sim 11$) and the epoch of observation becomes quite short. Over timescales of $400 - 500$ Myr, there would be just enough time to form an early galaxy population, build up its stellar mass, and eject heavy elements from its earliest supernovae into a region $\lesssim 100$ kpc in size. In this scenario there could be large metal-free regions of the IGM, but C IV observations at present sensitivities would only probe the regions where local production was important. In time, IR spectra with higher resolution and SNR should be able to track the evolution of weaker C IV lines in the tenuous IGM, and these systems will provide a more sensitive test of local versus gloal enrichment scenarios in the early universe.

I would like to extend special thanks to the Gemini Observatory staff, and particularly Dick Joyce, for their assistance in planning and executing the observations presented here. Thanks as well to Hsiao-Wen Chen for providing the code used for the curve-of-growth analysis, and to George Becker and Wal Sargent for allowing use of their optical spectrum of SDSS1030+0524. Thanks to Scott Burles and John O'Meara for advice on the data reduction and interpretation, and to Romeel Davé and Ben Oppenheimer for interesting discussions about this work's relationship to their numerical simulations. The data for this program were obtained through Gemini allocations GS-2005A-Q-4 and GS-2006A-Q-9. The research was supported with funds from the Pappalardo Fellowships in Physics program at MIT, and an AAS small research grant.

REFERENCES

Adelberger, K. L., Steidel, C. C., Shapley, A. E., & Pettini, M. 2003, ApJ, 584, 45

Calzetti, D., Kinney, A. L., & Storchi-Bergmann, T. 1994, ApJ, 429, 582

Djorgovski, S. G., Castro, S., Stern, D., & Mahabal, A. A. 2001, ApJ, 560, L5

Elias, J. H., Vukobratovich, D., Andrew, J. R., Cho, M. K., Cuberly, R. W., Don, K., Gerzoff, A., Harmer, C. F., Harris, D., Heynssens, J. B., Hicks, J., Kovacs, A., Li, C., Liang, M., Moon, I. K., Pearson, E. T., Plum, G., Roddier, N. A., Tvedt, J., Wolff, R. J., & Wong, W.-Y. 1998, in Proc. SPIE Vol. 3354, p. 555-565, Infrared Astronomical Instrumentation, Albert M. Fowler; Ed., ed. A. M. Fowler, 555–565

Fan, X., Hennawi, J. F., Richards, G. T., Strauss, M. A., Schneider, D. P., Donley, J. L., Young, J. E., Annis, J., Lin, H., Lampeitl, H., Lupton, R. H., Gunn, J. E., Knapp, G. R., Brandt, W. N., Anderson, S., Bahcall, N. A., Brinkmann, J., Brunner, R. J., Fukugita, M., Szalay, A. S., Szokoly, G. P., & York, D. G. 2004, AJ, 128, 515

Fan, X., Narayanan, V. K., Lupton, R. H., Strauss, M. A., Knapp, G. R., Becker, R. H., White, R. L., Pentericci, L., Leggett, S. K., Haiman, Z., Gunn, J. E., Ivezić, Ž., Schneider, D. P., Anderson, S. F., Brinkmann, J., Bahcall, N. A., Connolly, A. J., Csabai, I., Doi, M., Fukugita, M., Geballe, T., Grebel, E. K., Harbeck, D., Hennessy, G., Lamb, D. Q., Miknaitis, G., Munn, J. A., Nichol, R., Okamura, S., Pier, J. R., Prada, F., Richards, G. T., Szalay, A., & York, D. G. 2001, AJ, 122, 2833

Fan, X., Narayanan, V. K., Strauss, M. A., White, R. L., Becker, R. H., Pentericci, L., & Rix, H. 2002, AJ, 123, 1247

Fan, X., Strauss, M. A., Richards, G. T., Hennawi, J. F., Becker, R. H., White, R. L., Diamond-Stanic, A. M., Donley, J. L., Jiang, L., Kim, J. S., Vestergaard, M., Young, J. E., Gunn, J. E., Lupton, R. H., Knapp, G. R., Schneider, D. P., Brandt, W. N., Bahcall, N. A., Barentine, J. C., Brinkmann, J., Brewington, H. J., Fukugita, M., Harvanek, M., Kleinman, S. J., Krzesinski, J., Long, D., Neilsen, E. H., Nitta, A., Snedden, S. A., & Voges, W. 2006, AJ, 131, 1203

Fan, X., Strauss, M. A., Schneider, D. P., Becker, R. H., White, R. L., Haiman, Z., Gregg, M., Pentericci, L., Grebel, E. K., Narayanan, V. K., Loh, Y.-S., Richards, G. T., Gunn, J. E., Lupton, R. H., Knapp, G. R., Ivezić, Ž., Brandt, W. N., Collinge, M., Hao, L., Harbeck, D., Prada, F., Schaye, J., Strateva, I., Zakamska, N., Anderson, S., Brinkmann, J., Bahcall, N. A., Lamb, D. Q., Okamura, S., Szalay, A., & York, D. G. 2003, AJ, 125, 1649

Ferland, G. J., Korista, K. T., Verner, D. A., Ferguson, J. W., Kingdon, J. B., & Verner, E. M. 1998, PASP, 110, 761

Giavalisco, M., Dickinson, M., Ferguson, H. C., Ravindranath, S., Kretchmer, C., Moustakas, L. A., Madau, P., Fall, S. M., Gardner, J. P., Livio, M., Papovich, C., Renzini, A., Spinrad, H., Stern, D., & Riess, A. 2004, ApJ, 600, L103

Grevesse, N. & Sauval, A. J. 1998, Space Science Reviews, 85, 161

Haardt, F. & Madau, P. 2001, in Clusters of Galaxies and the High Redshift Universe Observed in X-rays

Leitherer, C., Schaerer, D., Goldader, J. D., Delgado, R. M. G., Robert, C., Kune, D. F., de Mello, D. F., Devost, D., & Heckman, T. M. 1999, ApJS, 123, 3

McDonald, P. & Miralda-Escudé, J. 2001, ApJ, 549, L11

O'Meara, J. M., Tytler, D., Kirkman, D., Suzuki, N., Prochaska, J. X., Lubin, D., & Wolfe, A. M. 2001, ApJ, 552, 718

Oppenheimer, B. D. & Davé, R. 2006, ArXiv Astrophysics e-prints

Pettini, M., Madau, P., Bolte, M., Prochaska, J. X., Ellison, S. L., & Fan, X. 2003, ApJ, 594, 695

Rauch, M., Sargent, W. L. W., Womble, D. S., & Barlow, T. A. 1996, ApJ, 467, L5+

Rousselot, P., Lidman, C., Cuby, J.-G., Moreels, G., & Monnet, G. 2000, A&A, 354, 1134

Schaye, J., Aguirre, A., Kim, T., Theuns, T., Rauch, M., & Sargent, W. L. W. 2003, ApJ, 596, 768

Scott, J., Bechtold, J., Dobrzycki, A., & Kulkarni, V. P. 2000, ApJS, 130, 67

Shapley, A. E., Steidel, C. C., Adelberger, K. L., Dickinson, M., Giavalisco, M., & Pettini, M. 2001, ApJ, 562, 95

Simcoe, R. A., Sargent, W. L. W., & Rauch, M. 2004, ApJ, 606, 92

Simcoe, R. A., Sargent, W. L. W., Rauch, M., & Becker, G. 2006, ApJ, 637, 648

Songaila, A. 2001, ApJ, 561, L153

—. 2005, AJ, 130, 1996

—. 2006, AJ, 131, 24

Spergel, D. N., Bean, R., Dore', O., Nolta, M. R., Bennett, C. L., Hinshaw, G., Jarosik, N., Komatsu, E., Page, L., Peiris, H. V., Verde, L., Barnes, C., Halpern, M., Hill, R. S., Kogut, A., Limon, M., Meyer, S. S., Odegard, N., Tucker, G. S., Weiland, J. L., Wollack, E., & Wright, E. L. 2006, ArXiv Astrophysics e-prints

Steidel, C. C., Adelberger, K. L., Giavalisco, M., Dickinson, M., & Pettini, M. 1999, ApJ, 519, 1

Storrie-Lombardi, L. J., McMahon, R. G., & Irwin, M. J. 1996, MNRAS, 283, L79

Thompson, R. I., Eisenstein, D., Fan, X., Dickinson, M., Illingworth, G., & Kennicutt, R. C. 2006, ArXiv Astrophysics e-prints

White, R. L., Becker, R. H., Fan, X., & Strauss, M. A. 2003, AJ, 126, 1

TABLE 1
C IV Lines Detected Toward SDSS1306+0356

$z_{\rm C\ IV}$	σ_z	$W_{\rm r,1548}$	σ_W	$W_{\rm r,1551}$	σ_W	EW Ratio	$\sigma_{\rm ratio}$	$\log(N_{\rm C\ IV})$	$N_{\rm comp}$
5.45153	0.00015	104	14	42	13	2.48	0.82	13.15	2
5.67430	0.00011	155	16	134	21	1.17	0.22	14.30	1
5.92718	0.00011	80	11	30	4	2.72	0.54	12.90	2

TABLE 2
C IV Lines Detected Toward SDSS1030+0524

$z_{\rm C\ IV}$	σ_z	$W_{\rm r,1548}$	σ_W	$W_{\rm r,1551}$	σ_W	EW Ratio	$\sigma_{\rm ratio}$	$\log(N_{\rm C\ IV})$	$N_{\rm comp}$
5.45886	0.00015	181	29	117	19	1.54	0.35	13.65	2
5.73318	0.00005	254	13	≤ 197	14	≥ 1.29	0.11	13.85	2
5.74313	0.00008	≤ 164	13	117	12	≤ 1.41	0.19	14.10	1
5.82374	0.00005	288	12	160	13	1.80	0.17	13.15	6
5.82791	0.00007	263	19	155	17	1.69	0.22	13.40	4
5.83013	0.00007	257	16	146	15	1.76	0.21	13.30	4
5.97594	0.00018	68	11	40	10	1.67	0.48	13.40	1
6.13479	0.00017	65	9	26	9	2.48	0.97	13.30	1
6.17568	0.00018	54	8	49	12	1.09	0.31	13.30	1

TABLE 3
C IV Column Density Distribution by Redshift

		$\log(N_{\rm C\ IV})$							
		$13.00-13.75$				$13.75-14.50$			
Δz	$\Delta X_{\rm full}$[1]	$f_{\rm comp}$[2]	$\Delta X_{\rm eff}$[3]	$N_{\rm lines}$	$\log f(N_{\rm C\ IV})$[4]	$f_{\rm comp}$	$\Delta X_{\rm eff}$	$N_{\rm lines}$	$\log f(N_{\rm C\ IV})$
5.40-5.72	2.98	0.193,0.084	0.412	1	-13.27	0.624,0.345	1.440	2	-14.27
5.72-6.21	3.35	0.500,0.318	1.247	4	-13.16	0.880,0.709	2.546	3	-14.34
5.90-6.21	1.64	0.379,0.350	0.578	4	-12.83	0.848,0.694	1.162	0	< -14.48

[1]Full absorption path (defined by Equation 1) along redshift range assuming 100% sample completeness.
[2]Compleness along each sightline for given range in redshift and $N_{\rm C\ IV}$. First value is for SDSS1306+0356, second is for SDSS1030+0524.
[3]Effective redshift path for bin, determined by applying the corrections given in previous column.
[4]Column density distribution function value.